Regularity as Intrinsic Reward for Free Play

Cansu Sancaktar
Max Planck Institute for Intelligent Systems
Tübingen, Germany
cansu.sancaktar@tuebingen.mpg.de

Justus Piater
University of Innsbruck
Innsbruck, Austria
justus.piater@uibk.ac.at

Georg Martius
Uni-Tübingen & Max Planck Institute for Intelligent Systems
Tübingen, Germany
georg.martius@uni-tuebingen.de

Abstract

We propose regularity as a novel reward signal for intrinsically-motivated reinforcement learning. Taking inspiration from child development, we postulate that striving for structure and order helps guide exploration towards a subspace of tasks that are not favored by naive uncertainty-based intrinsic rewards. Our generalized formulation of Regularity as Intrinsic Reward (RaIR) allows us to operationalize it within model-based reinforcement learning. In a synthetic environment, we showcase the plethora of structured patterns that can emerge from pursuing this regularity objective. We also demonstrate the strength of our method in a multi-object robotic manipulation environment. We incorporate RaIR into free play and use it to complement the model's epistemic uncertainty as an intrinsic reward. Doing so, we witness the autonomous construction of towers and other regular structures during free play, which leads to a substantial improvement in zero-shot downstream task performance on assembly tasks.[1]

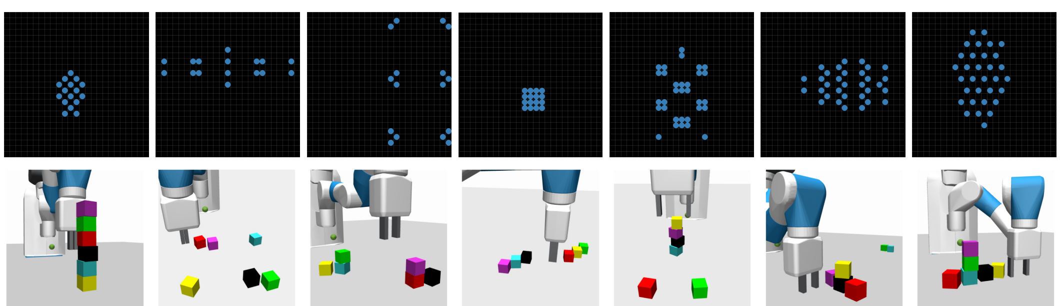

Figure 1: **Regularity as intrinsic reward yields ordered and symmetric patterns.** In SHAPEGRIDWORLD (top row) and in CONSTRUCTION (bottom row), we showcase the generated constellations when maximizing our proposed regularity reward RaIR.

1 Introduction

Regularity, and symmetry as a specific form of regularity, are ubiquitous in nature as well as in our manufactured world. The ability to detect regularity helps to identify essential structures,

16th European Workshop on Reinforcement Learning (EWRL 2023).

[1]Videos are available at https://sites.google.com/view/rair-project.

minimizing redundancy and allowing for efficient interaction with the world [1]. Not only do we encounter symmetries in arts, design, and architecture, but our preference also showcases itself in play behavior. Adults and children have both been observed to prefer symmetry in visual perception, where symmetric patterns are more easily detected, memorized, and copied [2, 3]. Several works in developmental psychology show that regular patterns and symmetries are actively sought out during free play in children as well as adults [4–6].

Considering this in the context of a child's developmental cycle is intriguing. Studies show that children at the age of 2 exhibit a shift in their exploratory behavior. They progress from engaging in random actions on objects and unstable arrangements to purposefully engaging in functional activities and intentionally constructing stable configurations [7, 8, 5]. Bailey [4] reports that by 5 years of age, children build more structured arrangements out of blocks that exhibit alignment, balance, and examples of symmetries [5].

Despite the dominance of regularity in our perceptual systems and our preference for balance and stability during play, these principles are not yet well investigated within intrinsically-motivated reinforcement learning (RL). One prominent intrinsic reward definition is novelty, i.e. the agent is incentivized to visit areas of the state space with high expected information gain [9–12]. However, one fundamental problem with plain novelty-seeking objectives is that the search space is often unconstrained and too large. As an agent only has limited resources to allocate during play time, injecting appropriate inductive biases is crucial for sample efficiency, good coverage during exploration, and emergence of diverse behaviors. As proposed by Sancaktar et al. [12], using structured world models to inject a relational bias into exploration, yields more object and interaction-related novelty signals. However, which types of information to prioritize are not explicitly encoded in any of these methods. The direction of exploration is often determined by the inherent biases in the practical methods deployed. With imperfect world models that have a limited learning capacity and finite-horizon planning, novelty-seeking methods are observed to prefer "chaotic" dynamics, where small perturbations lead to diverging trajectories, such as throwing, flipping, and poking objects. This in turn means that behaviors focusing on alignment, balance, and stability are overlooked. Not only are these behaviors relevant, as shown in developmental psychology, they also enable expanding and diversifying the types of behavior uncovered during exploration. As the behaviors observed during exploration are highly relevant for being able to solve downstream tasks, a chaos-favoring exploration will make it hard to solve assembly tasks, such as stacking. Indeed, successfully solving assembly tasks with more than 2 objects has been a challenge for intrinsically-motivated reinforcement learning.

We pose the question: how can we define an intrinsic reward signal such that RL agents prefer structured and regular patterns? We propose RaIR: **R**egularity **a**s **I**ntrinsic **R**eward, which aims to achieve highly ordered states. Mathematically, we operationalize this idea using entropy minimization of a suitable state description. Entropy and symmetries have been linked before [13, 14], however, we follow a general notion of regularity, i.e. where patterns reoccur and thus their description exhibits high redundancy / low entropy. In this sense, symmetries are a consequence of being ordered [15]. Regularity also means that the description is compressible, which is an alternative formulation. As argued by Schmidhuber [16], aiming for compression-progress is a formidable curiosity signal, however, it is currently unclear how to efficiently predict and optimize for it.

After studying the design choices in the mathematical formulation of regularity and the relation to symmetry operations, we set out to evaluate our regularity measure in the context of model-based reinforcement learning/planning, as it allows for highly sample-efficient exploration and solving complex tasks zero-shot, as shown in Sancaktar et al. [12]. To get a clear understanding of RaIR, we first investigate the generated structures when directly planning to optimize it using the ground truth system dynamics. A plethora of patterns emerge that are highly *regular*, as illustrated in Fig. 1.

Our ultimate goal is, however, to inject the proposed regularity objective into a free-play phase, where a robot can explore its capabilities in a task-free setting. During this free play, the dynamics model is learned on-the-go. We build on CEE-US [12], a free-play method that uses an ensemble of graph neural networks as a structured world model and the model's epistemic uncertainty as the only intrinsic reward. The epistemic uncertainty is estimated by the ensemble disagreement and acts as an effective novelty-seeking signal. We obtain *structure-seeking free play* by combining the conventional novelty-seeking objective with RaIR.

Our goal is to operationalize regularity, which is a well-established concept in developmental psychology, within intrinsically motivated RL. Furthermore, we showcase that biasing information-

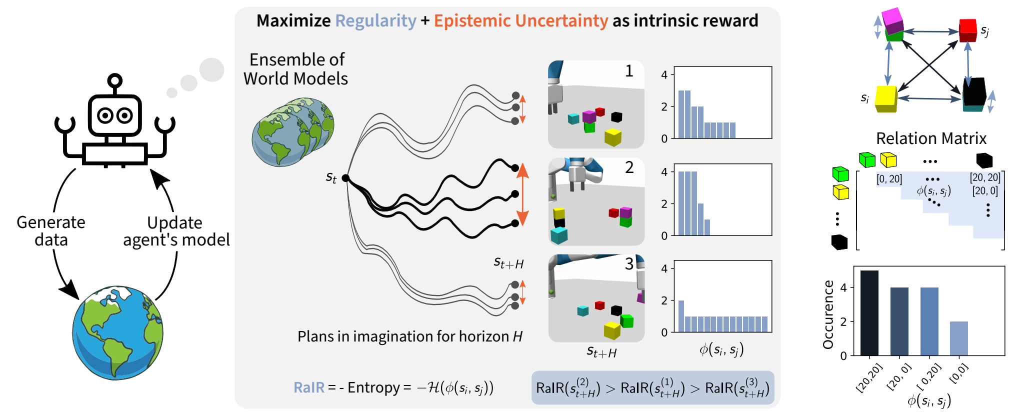

(a) RaIR + CEE-US: Regularity with Epistemic Uncertainty of Structured World Models (b) RaIR computation

Figure 2: **Regularity as intrinsic reward during free play.** (a) RaIR + CEE-US uses model-based planning to optimize H timesteps into the future for the combination of RaIR (Eq. 2) and epistemic uncertainty (ensemble disagreement of world models). (b) Here, for RaIR we use the absolute difference vector between objects: $\phi(s_i, s_j) = \{(|\lfloor s_{i,x} - s_{j,x}\rceil|, |\lfloor s_{i,y} - s_{j,y}\rceil|)\}$.

search towards regularity with RaIR indeed leads to the construction of diverse regular structures during play and significantly improves zero-shot performance in downstream tasks that also favor regularity, most notably assembly tasks. Besides conceptual work on compression [16, 17], to our knowledge, we are the first to investigate regularity as an intrinsic reward signal, bridging the gap between the diversity of behaviors observed in children's free play and what we can achieve with artificial agents.

2 Method

First, we introduce our intrinsic reward definition for regularity. Then, we present its practical implementation and explain how we combine this regularity objective into model learning within free play.

2.1 Preliminaries

In this work, we consider environments that can be described by a fully observable Markov Decision Process (MDP), given by the tuple $(\mathcal{S}, \mathcal{A}, f^a_{ss'}, r^a_{ss'})$, with the state-space $\mathcal{S} \in \mathbb{R}^{n_s}$, the action-space $\mathcal{A} \in \mathbb{R}^{n_a}$, the transition kernel $f : \mathcal{S} \times \mathcal{A} \to \mathcal{S}$, and the reward function r. Importantly, we consider the state-space to be factorized into the different entities, e.g. $\mathcal{S} = (\mathcal{S}_{\text{obj}})^N \times \mathcal{S}_{\text{robot}}$ for the state space of a robotic agent and N objects. We use model-based reinforcement learning, where data from interactions with the environment is used to learn a model $\tilde{f}$ of the MDP dynamics [18]. Using this model, we consider finite-horizon (H) optimization/planning for undiscounted cumulative reward:

$$\mathbf{a}^\star_t = \arg\max_{\mathbf{a}_t} \sum_{h=0}^{H-1} r(s_{t+h}, a_{t+h}, s_{t+h+1}), \tag{1}$$

where s_{t+h} are imagined states visited by rolling out the actions using $\tilde{f}$, which is assumed to be deterministic. The optimization of Eq. 1 is done with the improved Cross-Entropy Method (iCEM) [19] in a model predictive control (MPC) loop, i.e. re-planning after every step in the environment. Although this is not solving the full reinforcement learning problem (infinite horizon and stochastic environments), it is very powerful in optimizing for tasks on-the-fly and is thus suitable for optimizing changing exploration targets and solving downstream tasks zero-shot.

2.2 Regularity as Intrinsic Reward

Quite generally, regularity refers to the situation in which certain patterns reoccur. Thus, we formalize regularity as the **redundancy** in the description of the situation, to measure the degree of sub-structure recurrence. A decisive question is: which description should we use? Naturally, there is certain freedom in this choice, as there are many different coordinate frames. For instance, we could consider the list of absolute object positions or rather a relative representation of the scene.

To formalize, we define a mapping $\Phi : \mathcal{S} \to \{\mathcal{X}\}^+$ from state to a multiset $\{\mathcal{X}\}^+$ of symbols (e.g. coordinates). A multiset is a set where elements can occur multiple times, e.g. $\{a, a, b\}^+$. This multiset can equivalently be described by a tuple (X, m), where X is the set of the unique elements, and $m : X \to \mathbb{Z}^+$ is a function assigning the multiplicity, i.e. the number of occurrences $m(x)$ for the elements $x \in X$. For the previous example, we get $(\{a, b\}, \{a : 2, b : 1\})$. Given the multiset $(X, m) \in \{\mathcal{X}\}^+$, we define the discrete empirical distribution by the relative frequency of occurrence $p(x) = m(x)/\sum_{x' \in X} m(x')$ for $x \in X$, also referred to as a histogram.

We define the regularity reward metric using (negative) Shannon entropy [20] of this distribution as:

$$r_{\mathrm{RaIR}}(s) \coloneqq -\mathcal{H}(\Phi(s)) = \sum_{x \in X} p(x) \log p(x) \quad \text{with } (X, m) = \Phi(s), \quad p(x) = \frac{m(x)}{\sum\limits_{x' \in X} m(x')}. \tag{2}$$

We will now discuss concrete cases for the mapping Φ, i.e. how to describe a particular state.

Direct RaIR. In the simplest case, we describe the state s directly by the properties of each of the entities. For that, we define the function $\phi : \mathcal{S}_{\text{obj}} \to \{\mathcal{X}\}^+$, that maps each entity to a set of symbols and obtain $\Phi(s) = \uplus_{i=1}^{N} \phi(s_{\text{obj},i})$ as a union of all symbols. The symbols can be, for instance, discretized coordinates, colors, or other properties of the entities.

Let us consider the example where ϕ is extracting the object's Cartesian x and y coordinates in a rounded manner as $\phi(s) = \{\lfloor s_x \rceil, \lfloor s_y \rceil\}^+$, as shown in Fig. 3. The most irregular configuration would be when no two objects share the same rounded value in x and y. The object configuration becomes more and more regular the more objects share the same $\lfloor x \rceil$ and $\lfloor y \rceil$ coordinates. The most regular configuration is if all objects are in the same place. Note that this choice favors an axis-aligned configuration, and it is not invariant under global rotations.

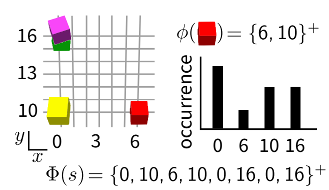

Figure 3: Illustration of direct RaIR for $\phi = \{\lfloor x \rceil, \lfloor y \rceil\}$.

Relational RaIR of order k. Our framework for regularity quantification can easily be extended to a relational perspective, where we don't compute the entropy over aspects of individual entity properties, but instead on their pairwise or higher-order **relations**. This means that for a k-order regularity measure, we are interested in tuples of k entities. Thus, the mapping function ϕ no longer takes single entities as input, but instead operates on k-tuples:

$$\phi : (\mathcal{S}_{\text{obj}})^k \to \{\mathcal{X}\}^+. \tag{3}$$

ϕ is a function that describes some relations between the k input entities by a set of symbols.

For k-order regularity, the multiset Φ, over which we compute the entropy, is now given by

$$\Phi^{(k)} = \bigcup_{\{i_1,\ldots,i_k\} \in \mathcal{P}} \phi(s_{\text{obj},i_1}, \ldots, s_{\text{obj},i_k}) \quad \text{with } \mathcal{P} = \mathrm{P}(\{1, \ldots, N\}, k) \tag{4}$$

merged from all k-permutations of the N entities, denoted as $\mathrm{P}(\{1, \ldots, N\}, k)$. In the case of a permutation invariant ϕ, Eq. 4 regards only the combinations $\mathrm{C}(\{1, \ldots, N\}, k)$. Note that direct RaIR is equivalent to the relational RaIR of order 1. Given the mapping Φ, the RaIR measure is computed as before with Eq. 2.

Depending on the order k and the function ϕ, we can select which regularities are going to be favored. Let us consider the example of a pair-wise relational RaIR ($k = 2$), where ϕ computes the relative positions: $\phi(s_i, s_j) = \{\lfloor s_i - s_j \rceil\}$, and rounding is performed elementwise. Whenever two entities have the same relative position to each other, the redundancy is detected. For $k = 3$ our regularity measure would be able to pick up sub-patterns composed of three objects, such as triangles and so forth.

As we are interested in physical interactions of the robot with objects and objects with objects, we choose RaIR of order $k = 2$ and explore various ϕ functions.

Table 1: **Properties of RaIR with different ϕ regarding symmetry operations**. The first block indicates to which operations RaIR is invariant, ignoring rounding (a.a.: axes aligned). The second block assesses whether a pattern, where the given symmetry operation maps several entities to another, has increased regularity. Rounding and absolute value are element-wise. Distance d is also rounded.

	invariant?				favored / increases RaIR?				
symmetry operation	direct $\phi = \lfloor s_i \rceil$	rel. pos $\lfloor s_i - s_j \rceil$	|rel. pos| $\lvert\lfloor s_i - s_j \rceil\rvert$	distance $\mathrm{d}(s_i, s_j)$	direct $\lfloor s_i \rceil$	rel. pos $\lfloor s_i - s_j \rceil$	|rel. pos| $\lvert\lfloor s_i - s_j \rceil\rvert$	distance $\mathrm{d}(s_i, s_j)$	Sym(∘) = •
translation	✗	✓	✓	✓	✗	✓	✓	✓	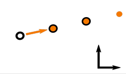
translation – a.a.	✓	✓	✓	✓	✓	✓	✓	✓	
rotation	✗	✓	✗	✓	✗	✗	✗	✓	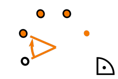
rotation – 90°	✓	✓	✓	✓	✗	✗	✓	✓	
reflection	✗	✓	✗	✓	✗	✗	✗	✓	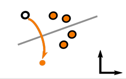
reflection – a.a.	✓	✓	✓	✓	✓	✗	✓	✓	
glide refl.	✗	✓	✗	✓	✗	✗$^{(1)}$	✗$^{(1)}$	✓	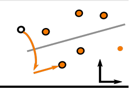
glide refl. – a.a.	✓	✓	✓	✓	✓	✗$^{(1)}$	✓	✓	

$^{(1)}$This is for one glide refl. operation. RaIR is increased for 2 glide refl. composition as it collapses onto transl.

2.2.1 Properties of RaIR with Pairwise Relations and Practical Implementation

For simplicity, we are considering in the following that ϕ maps to a single symbol. Then for pairwise relationships ($k = 2$), RaIR can be implemented using a relation matrix $F \in \mathcal{X}^{N \times N}$. The entries F_{ij} are given by $\phi(s_i, s_j)$ with $s_i, s_j \in S_{\text{obj}}$. After constructing the relation matrix, we need the histogram of occurrences of unique values in this matrix to compute the entropy (Eq. 2). For continuous state spaces, the mapping function needs to implement a discretization step, which we implement by a binning of size b. For simplicity of notation, we reuse the rounding notation $\lfloor \cdot \rceil$ for this discretization step. This bin size b determines the precision of the measured regularity. In practice, we do not apply ϕ on the full entity state space, but on a subspace that contains e.g. the x-y(-z) positions.

To understand the properties of our regularity measure for different ϕ, we present in Table 1 a categorization using the known symmetry operations in 2D and the following ϕ (applied to x-y positions): direct $\phi(s_i) = \lfloor s_i \rceil$(see previous section), relative position (difference vector) $\phi(s_i, s_j) = \lfloor s_i - s_j \rceil$, absolute value of the relative position[2] $\phi(s_i, s_j) = \lvert\lfloor s_i - s_j \rceil\rvert$, and Euclidean distance $\phi(s_i, s_j) = \lfloor \lVert s_i - s_j \rVert \rceil$. Figure 2b illustrates the RaIR computation using the absolute value of the relative position.

In Table 1, we first consider whether the measure is invariant under symmetry operations. That means if the value of RaIR stays unchanged when the entire configuration is transformed. We find that both Euclidean distance and relative position are invariant to all symmetry operations. The second and possibly more important question is whether a configuration with substructures of that symmetry has a higher regularity value than without, i.e. will patterns with these symmetries be favored. We find that Euclidean distance favors all symmetries, followed by absolute value of the relative position. A checkmark in this part of the table means that the more entities can be mapped to each other with the same transformation, the higher RaIR. Although the Euclidean distance seems favorable, we find that it mostly clumps entities and creates fewer alignments. To get a sense of the patterns scoring high in the regularity measure, Fig. 1 showcases situations that emerge when RaIR with absolute value of relative position is optimized (details below).

2.3 Regularity in Free Play

Our goal is to explicitly put the bias of regularity into free play via RaIR, as illustrated in Fig. 2a. What we want to achieve is not just that the agent creates regularity, but that it gathers valuable experience in creating regularity. This ideally leads to directing exploration towards patterns/arrangements that are novel.

[2]The rounding and the absolute value functions are applied coordinate wise.

We propose to use RaIR to augment plain novelty-seeking intrinsic rewards, in this work specifically ensemble disagreement. We choose ensemble disagreement because 1) we need a reward definition that allows us to predict future novelty, such that we can use it inside model-based planning (this constraint makes methods relying on retrospective novelty such as Intrinsic Curiosity Module (ICM) [10] ineligible), and 2) we want to use the models learned during free play for zero-shot downstream task generalization via planning in a follow-up extrinsic phase. It has been shown in previous works that guiding exploration by the model's own epistemic uncertainty, approximated via ensemble disagreement, leads to learning more robust world models compared to e.g. Random Network Distillation (RND) [21], resulting in improved zero-shot downstream task performance [12]. That is why we choose ensemble disagreement to compute expected future novelty.

We train an ensemble of world models $\{(\tilde{f}_{\theta m})_{m=1}^{M}\}$, where M denotes the ensemble size. The model's epistemic uncertainty is approximated by the disagreement of the ensemble members' predictions. The disagreement reward is given by the trace of the covariance matrix [12]:

$$r_{\text{Dis}} = \operatorname{tr}\big(\operatorname{Cov}(\{\hat{s}_{t+1}^{m} = \tilde{f}_{\theta m}(s_t, a_t) \mid m = 1, \dots, M\})\big). \tag{5}$$

We incorporate our regularity objective into free play by using a linear combination of RaIR and ensemble disagreement. Overall, we have the intrinsic reward:

$$r_{\text{intrinsic}} = r_{\text{RaIR}} + \lambda \cdot r_{\text{Dis}}, \tag{6}$$

where λ controls the trade-off between regularity and pure epistemic uncertainty.

Model-based Planning with Structured World Models To optimize the reward function on-the-fly, we use model-based planning using zero-order trajectory optimization, as introduced in Sec. 2.1. Concretely, we use CEE-US [12], which combines structured world models and epistemic uncertainty (Eq. 5) as intrinsic reward. The structured world models are ensembles of message-passing Graph Neural Networks (GNNs) [22], where each object corresponds to a node in the graph. The node attributes $\{s_{t,i} \in \mathcal{S}_{\text{obj}} \mid i = 1, \dots, N\}$ are the object features such as position, orientation, and velocity at time step t. The state representation of the actuated agent $s_{\text{robot}} \in \mathcal{S}_{\text{robot}}$ similarly contains position and velocity information about the robot. We treat the robot as a global node in the graph [12]. We refer to the combination of RaIR with ensemble disagreement, medium-horizon planning (20-30 time steps), and structured world models as RaIR + CEE-US (Fig. 2a).

3 Experiments

We evaluate RaIR in the two environments shown in Fig. 1.

ShapeGridWorld is a grid environment, where each circle represents an entity/agent that is controlled separately in x-y directions. Entities are controlled one at a time. Starting from time step $t = 0$, the entity with $i = 1$ is actuated for T time steps, where T is the entity persistency. Then, at $t = T$, actuation switches over to entity $i = 2$ and we keep iterating over the entities in this fashion. Each circle is treated as an entity/object for the regularity computation with a 2D-entity state space S_{obj} with x-y positions.

Fetch Pick & Place Construction is an extension of the Fetch Pick & Place environment [23] to more cubes [24] and a large table [12]. An end-effector-controlled robot arm is used to manipulate blocks. The robot state $S_{\text{robot}} \in \mathbb{R}^{10}$ contains the end-effector position and velocity and the gripper's state (open/close) and velocity. Each object's state $S_{\text{obj}} \in \mathbb{R}^{12}$ is given by its pose and velocities. For free play, we use 6 objects and consider several downstream tasks with varying object numbers.

3.1 Emerging Patterns in ShapeGridWorld and Construction with RaIR

To get a sense of what kinds of patterns emerge following our regularity objective with RaIR, we do planning using ground truth (GT) models, i.e. with access to the true simulator itself for planning. We perform these experiments to showcase that we can indeed get *regular* constellations with our proposed formulation. Since we can perform multi-horizon planning without any accumulating model errors using ground truth models, we can better investigate the global/local optima of our regularity reward. Note that as we are using a zero-order trajectory optimizer with a limited sample budget and finite-horizon planning, we don't necessarily converge to the global optima. We use

$\phi(s_i, s_j) = \{(|\lfloor s_{i,x} - s_{j,x} \rceil|, |\lfloor s_{i,y} - s_{j,y} \rceil|)\}$ for RaIR in both environments. The emerging patterns are shown in Fig. 1.

In the 2D SHAPEGRIDWORLD environment, we indeed observe that regular patterns with translational, reflectional (axis-aligned), glide-reflectional (axis-aligned), and rotational symmetries emerge (see top row in Fig. 1).

For CONSTRUCTION, we also observe complex constellations with regularities, even stacks of all 6 objects (see bottom row in Fig. 1). Since we are computing RaIR on the x-y positions, a stack of 6 is the global optimum. The optimization of RaIR for this case is shown in Fig. 4. Note that stacking itself is a very challenging task, and was so far only reliably achievable with reward shaping or tailored learning curricula [24]. The fact that these constellations appear naturally from our regularity objective, achievable with a planning horizon of 30 timesteps, is by itself remarkable.

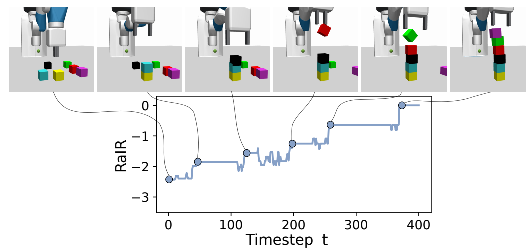

Figure 4: **RaIR throughout a rollout** starting from a random initial configuration when optimizing only for regularity with the GT model.

Additional example patterns generated in CONSTRUCTION with RaIR on the x-y-z positions can be found in the Suppl. A. In that case, a horizontal line on the ground and a vertical line into air, i.e. a stack, are numerically equivalent with respect to RaIR. Choosing to operate on the x-y-subspace is injecting the direction of gravity and provides a bias towards vertical alignments.

3.2 Free Play with RaIR in CONSTRUCTION

We perform free play in CONSTRUCTION, i.e. only optimize for intrinsic rewards, where we learn models on-the-go. During free play, we start with randomly initialized models and an empty replay buffer. Each iteration of free play consists of data collection with environment interactions (via online planning), and then model training on the collected data so far (offline).

In each iteration of free play, we collect 2000 samples (20 rollouts with 100 timesteps each) and add them to the replay buffer. During the online planning part for data collection, we only perform inference with the models and no training is performed. Afterwards, we train the model for a fixed number of epochs on the replay buffer. We then continue with data collection in the next free play iteration. More details can be found in Suppl. E.

For this intrinsic phase, we combine our regularity objective with ensemble disagreement as per Eq. 6. The goal is to bias exploration and the search for information gain towards regular structures, corresponding to the optima that emerge with ground truth models, as shown in Fig. 1.

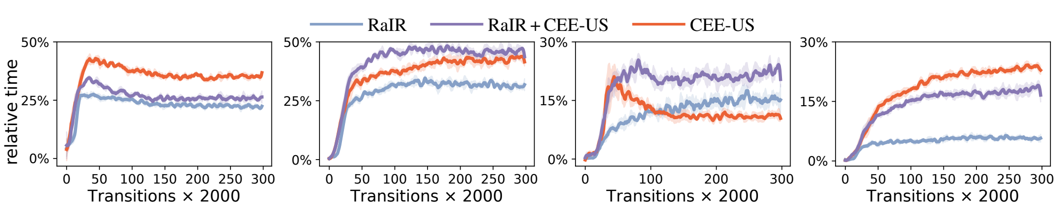

(a) 1 object moves (b) 2 or more objects move (c) object(s) in air (d) object(s) flipped

Figure 5: **Comparison of interactions during free play in CONSTRUCTION** when combining ensemble disagreement with RaIR (with $\lambda = 0.1$) compared to CEE-US and pure RaIR. These metrics count the relative amount of time steps that the agent performs certain types of interactions during free-play exploration . (a) *1 object moves* checks the amount of time the agent spends moving only one object at a time. Here, e.g. 50% metric indicates that an object was moved in 1K transitions of the overall 2K transitions collected in that free play iteration. (b) *2 or more objects move* checks if at least 2 objects are moving at the same time. (c) *Object(s) in air* means one or more objects are in air (including being held in air by the agent or being on top of another block). (d) *Object(s) flipped* checks for angular velocities above a threshold for one or more objects, i.e. if they are rolled/flipped. We used 5 independent seeds.

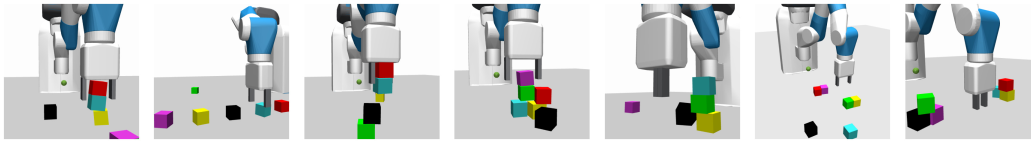

Iteration 251 Iteration 255 Iteration 259 Iteration 275 Iteration 284 Iteration 286 Iteration 296

Figure 6: **Snapshots from free play with RaIR + CEE-US.** We showcase snapshots of highest RaIR values, equivalent to lowest entropy, from exemplary rollouts at different iterations of free play. Following the regularity objective, stacks and alignments are generated.

In Figure 5, we analyze the quality of data generated during free play, in terms of observed interactions, for RaIR + CEE-US with the augmentation weight $\lambda = 0.1$, a pure RaIR run with no information-gain component in the intrinsic reward ($\lambda = 0$) and CEE-US.

For pure RaIR, we observe a decrease in the generated interactions. This has two reasons: 1) RaIR only aims to generate structure and the exploration problem is not solved, 2) once the controller finds a plan that leads to an optimum, even if it is local, there is no incentive to destroy it, unless a plan that results in better regularity can be found within the planning horizon. There is no discrimination between "boring" and "interesting" patterns with respect to the model's current capabilities. This in turn means that the robot creates e.g. a (spaced) line, which is a local optimum for RaIR, and then spends the rest of the episode, not touching any objects to keep the created alignment intact. With the injection of some disagreement in RaIR + CEE-US, we observe improved interaction metrics throughout free play in terms of 2 or more object interactions and objects being in the air (either being lifted by the robot or being stacked on top of another block). In practice, since the ensemble of models tends to hallucinate due to imperfect predictions, even for pure RaIR we observe dynamic pattern generations, as reflected in the interaction metrics (more details in Suppl. C).

Another reason why disagreement is helpful is due to the step-wise landscape of RaIR as shown in Fig. 4. Here, combining RaIR with ensemble disagreement effectively helps smoothen this reward function, making it easier to find plans with improvements in regularity with imperfect world models. For the plain disagreement case with CEE-US, more flipping behavior, and less air time are observed during free play, since the agent favors chaos. In Fig. 7, we report the highest achieved RaIR value in the collected rollouts throughout free play. We observe that RaIR + CEE-US indeed finds more regular structures during play, some of which are illustrated in Fig. 6. Results for $\phi(s_i, s_j) = \lfloor s_i - s_j \rceil$ can be found in Suppl. B.

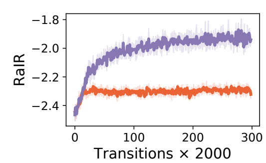

Figure 7: **Highest RaIR value throughout free play** for RaIR + CEE-US and CEE-US.

3.3 Zero-shot Generalization to Assembly Downstream Tasks with RaIR in Construction

After the fully-intrinsic free-play phase, we evaluate zero-shot generalization performance on downstream tasks, where we perform model-based planning with the learned world models. Note that now instead of optimizing for intrinsic rewards, we are optimizing for extrinsic reward functions r_{task} given by the environment (Suppl. F.4.1).

In Fig. 8, we present the evolution of success rates of models checkpointed throughout free play on the following assembly tasks: singletower with 3 objects, 2 multitowers with 2 objects each, pyramid with 5 and 6 objects. The combination RaIR + CEE-US yields significant improvements in the success rates of assembly tasks, as shown in Fig. 8 and Table 2. As we are biasing exploration towards regularity, we see a decrease in more chaotic interactions during play time, which is correlated with a decrease in performance for the more chaotic throwing and flipping tasks. For the generic Pick & Place task, we observe comparable performance.

3.4 Re-creating existing structures with RaIR

We test whether we can re-create existing arrangements in the environment with RaIR. If there are regularities / sub-structures already present in the environment, then completing or re-creating these patterns naturally becomes an optimum for RaIR, as repeating this pattern introduces redundancy, with multiple entries in the relation matrix repeated, corresponding to lower entropy.

Table 2: **Zero-shot downstream task generalization performance of RaIR + CEE-US vs. CEE-US** for assembly tasks as well as the generic pick & place task and the more chaos-oriented throwing and flipping. Results are shown for five independent seeds. In the bottom row, we report the success rates achieved via planning with ground truth models. This is to provide a baseline for how hard the task is to solve with finite-horizon planning and potentially suboptimally designed task rewards.

	Singletower 3	Multitower 2+2	Pyramid 5	Pyramid 6	Pick&Place 6	Throw 4	Flip 4
RaIR + CEE-US	$\mathbf{0.75 \pm 0.07}$	$\mathbf{0.77 \pm 0.06}$	$\mathbf{0.49 \pm 0.06}$	$\mathbf{0.18 \pm 0.04}$	$\mathbf{0.90 \pm 0.02}$	0.32 ± 0.02	0.63 ± 0.08
CEE-US	0.40 ± 0.12	0.52 ± 0.05	0.14 ± 0.09	0.02 ± 0.01	$\mathbf{0.90 \pm 0.02}$	$\mathbf{0.49 \pm 0.05}$	$\mathbf{0.73 \pm 0.1}$
GT	0.99	0.97	0.82	0.81	0.99	0.97	1.0

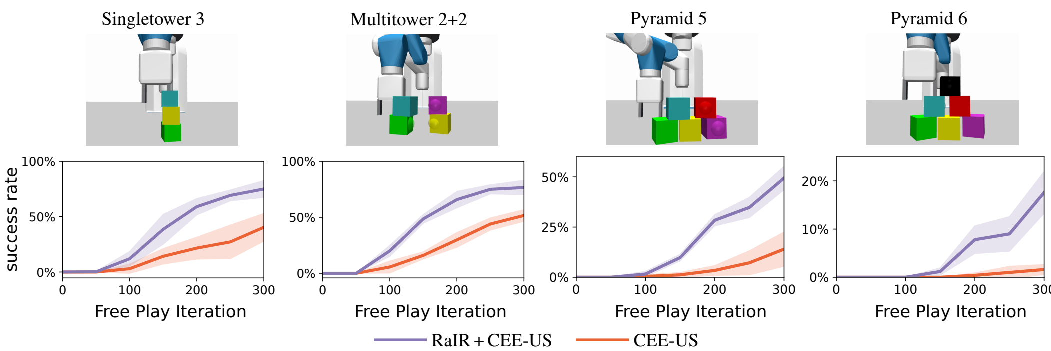

Figure 8: **Success rates for zero-shot downstream task generalization for assembly tasks** in CONSTRUCTION for model checkpoints over the course of free play. We compare RaIR + CEE-US ($\lambda = 0.1$) with CEE-US. We used five independent seeds.

We initialize pyramids, single- and multitowers out of the robot's manipulability range in CONSTRUCTION. We then plan using iCEM to maximize RaIR with GT models. Doing so, the agent manages to re-create the existing structures in the environment with the blocks it has within reach. Without the need to define any explicit reward functions, we can simply use our regularity objective to mimic existing ordered constellations. In Fig. 9, this is showcased for a pyramid with 3 objects, where in 15 rollouts a pyramid is recreated in 73% of the cases. More details can be found in Suppl. D.

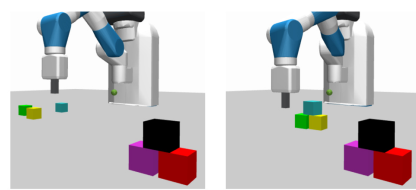

(a) $t = 0$ (b) $t = 200$

Figure 9: A pyramid initialized outside of the robot's reach is re-created by optimizing for RaIR.

4 Related Work

Intrinsic motivation in RL uses minimizing novelty/surprise to dissolve cognitive disequilibria as a prominent intrinsic reward signal definition [25, 9, 26–30]. As featured in this work, using the disagreement of an ensemble of world models as an estimate of expected information gain is a widely-used metric as it allows planning into the future [10–12]. Other prominent intrinsic rewards deployed in RL include learning progress [25, 31, 29], empowerment [32, 33] and maximizing for state space coverage with count-based methods [34, 35] and RND [21]. Another sub-category would be goal-conditioned unsupervised exploration methods combined with e.g. ensemble disagreement [36, 37] or asymmetric self-play [38].

Compression and more specifically compression progress have been postulated as driving forces in human curiosity by Schmidhuber [16]. However, the focus has been on the temporal aspect of compression, where it is argued that short and simple explanations of the past make long-horizon planning easier. In our work, we don't focus on compression in the temporal dimension, i.e. sequences of states. Instead, we perform compression as entropy minimization (in the relational case, equivalent to lossy compression) at a given timestep t, where we are interested in the relational redundancies in the current scene.

Assembly Tasks in RL with 3+ objects pose an open challenge, where most methods achieve stacking via tailored learning curricula with more than 20 million environment steps [24, 39], expert demonstrations [40], also together with high-level actions [41]. Hu et al. [36] manage to solve 3-object stacking in an unsupervised setting with goal-conditioned RL, using a very similar robotic setup to ours, but only with 30% success rate.

5 Discussion

Although the search for regularity and symmetry has been studied extensively in developmental psychology, these concepts haven't been featured within reinforcement learning yet. In this work, we propose a mathematical formulation of regularity as an intrinsic reward signal and operationalize it within model-based RL. We show that with our formulation of regularity, we indeed manage to create regular and symmetric patterns in a 2D grid environment as well as in a challenging compositional object manipulation environment. We also provide insights into the different components of RaIR and deepen the understanding of the types of regularities emerging from using different mappings ϕ. In the second part of the work, we incorporate RaIR within free play. Here, our goal is biasing information-search during exploration towards regularity. We provide a proof-of-concept that augmenting epistemic uncertainty-based intrinsic rewards with RaIR helps exploration for symmetric and ordered arrangements. Finally, we also show that our regularity objective can simply be used to imitate existing regularities in the environment.

Limitations Currently, we are restricted to fully-observable MDPs. We embrace object-centric representations as a suitable inductive bias in RL, where the observations per object (consisting of poses and velocities) are naturally disentangled. We also assume that this state space is interpretable such that we take, for instance, only the positions. In principle, ϕ could also be a learned mapping to a latent space. Applying RaIR directly to latent representations that are not inherently disentangled presents a challenge: developing a representation mirroring human-relevant structure and regularities. Here, examples of significant regular situations of interest could come in to learn a tokenizable representation for RaIR. This resembles real-world learning, where exposure to regular structures (e.g., towers, bridges) leads us to replicate these patterns while e.g. interacting with blocks. We leave this for future work. As we use finite-horizon planning, we don't necessarily converge to global optima. This can both be seen as a limitation and a feature, as it naturally allows us to obtain different levels of regularity in the generated patterns.

Acknowledgments and Disclosure of Funding

The authors thank Sebastian Blaes, Anselm Paulus, Marco Bagatella and Núria Armengol Urpí for helpful discussions and for their help reviewing the manuscript. The authors thank the International Max Planck Research School for Intelligent Systems (IMPRS-IS) for supporting Cansu Sancaktar. Georg Martius is a member of the Machine Learning Cluster of Excellence, EXC number 2064/1 – Project number 390727645. We acknowledge the financial support from the German Federal Ministry of Education and Research (BMBF) through the Tübingen AI Center (FKZ: 01IS18039B). This work was supported by the Volkswagen Stiftung (No 98 571).

References

[1] Yanxi Liu, Hagit Hel-Or, Craig S Kaplan, Luc Van Gool, et al. Computational symmetry in computer vision and computer graphics. *Foundations and Trends® in Computer Graphics and Vision*, 5(1–2):1–195, 2010.

[2] Fred Attneave. Symmetry, information, and memory for patterns. *The American journal of psychology*, 68(2):209–222, 1955.

[3] Marc H Bornstein, Kay Ferdinandsen, and Charles G Gross. Perception of symmetry in infancy. *Developmental psychology*, 17(1):82, 1981.

[4] Marjory W Bailey. A scale of block constructions for young children. *Child Development*, 4(2): 121–139, 1933.

[5] William A Zingrone. The construction of symmetry in children and adults. *The Journal of genetic psychology*, 175(2):91–104, 2014.

[6] Claire Golomb. The development of compositional strategies in children's drawings. *Visual Arts Research*, pages 42–52, 1987.

[7] Eleanor J Gibson. Exploratory behavior in the development of perceiving, acting, and the acquiring of knowledge. *Annual review of psychology*, 39(1):1–42, 1988.

[8] Jonas Langer. *The origins of logic: One to two years*. Academic Press, 1986. ISBN 978-0124365551.

[9] Deepak Pathak, Pulkit Agrawal, Alexei A. Efros, and Trevor Darrell. Curiosity-driven exploration by self-supervised prediction. In *International Conference on Machine Learning (ICML)*, 2017. URL https://proceedings.mlr.press/v70/pathak17a.html.

[10] Deepak Pathak, Dhiraj Gandhi, and Abhinav Gupta. Self-supervised exploration via disagreement. In *International Conference on Machine Learning (ICML)*, 2019. URL https://proceedings.mlr.press/v97/pathak19a.html.

[11] Ramanan Sekar, Oleh Rybkin, Kostas Daniilidis, Pieter Abbeel, Danijar Hafner, and Deepak Pathak. Planning to explore via self-supervised world models. In *International Conference on Machine Learning (ICML)*, 2020. URL https://proceedings.mlr.press/v119/sekar20a.html.

[12] Cansu Sancaktar, Sebastian Blaes, and Georg Martius. Curious exploration via structured world models yields zero-shot object manipulation. In *Advances in Neural Information Processing Systems (NeurIPS)*, 2022.

[13] Shu-Kun Lin. Correlation of entropy with similarity and symmetry. *Journal of Chemical Information and Computer Sciences*, 36(3):367–376, 1996.

[14] Daniel Lazarev. Information measures for entropy and symmetry. *arXiv preprint arXiv:2211.14857*, 2022.

[15] Edward Bormashenko. Entropy, information, and symmetry; ordered is symmetrical, ii: system of spins in the magnetic field. *Entropy*, 22(2):235, 2020.

[16] Jürgen Schmidhuber. Driven by compression progress: A simple principle explains essential aspects of subjective beauty, novelty, surprise, interestingness, attention, curiosity, creativity, art, science, music, jokes. In *Anticipatory Behavior in Adaptive Learning Systems: From Psychological Theories to Artificial Cognitive Systems 4*, pages 48–76. Springer, 2009. Longer preprint: https://arxiv.org/abs/0812.4360.

[17] Jürgen Schmidhuber. Powerplay: Training an increasingly general problem solver by continually searching for the simplest still unsolvable problem. *Frontiers in Psychology*, 4:313, 2013.

[18] Kurtland Chua, Roberto Calandra, Rowan McAllister, and Sergey Levine. Deep reinforcement learning in a handful of trials using probabilistic dynamics models. In *Advances in Neural Information Processing Systems (NeurIPS)*, 2018. URL https://proceedings.neurips.cc/paper_files/paper/2018/file/3de568f8597b94bda53149c7d7f5958c-Paper.pdf.

[19] Cristina Pinneri, Shambhuraj Sawant, Sebastian Blaes, Jan Achterhold, Joerg Stueckler, Michal Rolinek, and Georg Martius. Sample-efficient cross-entropy method for real-time planning. In *Conference on Robot Learning (CoRL)*, 2020. URL https://proceedings.mlr.press/v155/pinneri21a.html.

[20] Claude E Shannon. A mathematical theory of communication. *The Bell system technical journal*, 27(3):379–423, 1948.

[21] Yuri Burda, Harrison Edwards, Amos Storkey, and Oleg Klimov. Exploration by random network distillation. In *International Conference on Learning Representations (ICLR)*, 2019. URL https://openreview.net/forum?id=H1lJJnR5Ym.

[22] Peter W. Battaglia, Jessica B. Hamrick, Victor Bapst, Alvaro Sanchez-Gonzalez, Vinicius Zambaldi, Mateusz Malinowski, Andrea Tacchetti, David Raposo, Adam Santoro, Ryan Faulkner, Caglar Gulcehre, Francis Song, Andrew Ballard, Justin Gilmer, George Dahl, Ashish Vaswani, Kelsey Allen, Charles Nash, Victoria Langston, Chris Dyer, Nicolas Heess, Daan Wierstra, Pushmeet Kohli, Matt Botvinick, Oriol Vinyals, Yujia Li, and Razvan Pascanu. Relational inductive biases, deep learning, and graph networks. *arXiv:1806.01261*, 2018. URL https://arxiv.org/abs/1806.01261.

[23] Matthias Plappert, Marcin Andrychowicz, Alex Ray, Bob McGrew, Bowen Baker, Glenn Powell, J. Schneider, Joshua Tobin, Maciek Chociej, P. Welinder, V. Kumar, and W. Zaremba. Multi-goal reinforcement learning: Challenging robotics environments and request for research. *arXiv preprint arXiv:1802.09464*, 2018. URL https://arxiv.org/abs/1802.09464.

[24] Richard Li, Allan Jabri, Trevor Darrell, and Pulkit Agrawal. Towards practical multi-object manipulation using relational reinforcement learning. In *2020 IEEE International Conference on Robotics and Automation (ICRA)*, pages 4051–4058. IEEE, 2020. URL https://arxiv.org/abs/1912.11032.

[25] Jürgen Schmidhuber. A possibility for implementing curiosity and boredom in model-building neural controllers. In *Proceedings of the International Conference on Simulation of Adaptive Behavior: From Animals to Animats*, 1991. URL https://dl.acm.org/doi/10.5555/116517.116542.

[26] Kuno Kim, Megumi Sano, Julian De Freitas, Nick Haber, and Daniel Yamins. Active world model learning with progress curiosity. In *International Conference on Machine Learning (ICML)*, 2020. URL https://arxiv.org/abs/2007.07853.

[27] Oliver Groth, Markus Wulfmeier, Giulia Vezzani, Vibhavari Dasagi, Tim Hertweck, Roland Hafner, Nicolas Heess, and Martin Riedmiller. Is curiosity all you need? on the utility of emergent behaviours from curious exploration. *arXiv preprint arXiv:2109.08603*, 2021. URL https://arxiv.org/abs/2109.08603.

[28] J. Storck, S. Hochreiter, and J. Schmidhuber. Reinforcement driven information acquisition in non-deterministic environments. In *Proceedings of the International Conference on Artificial Neural Networks*, pages 159–164, Paris, 1995. EC2 & Cie. URL https://people.idsia.ch/~juergen/icann95new.pdf.

[29] Sebastian Blaes, Marin Vlastelica, Jia-Jie Zhu, and Georg Martius. Control What You Can: Intrinsically motivated task-planning agent. In *Advances in Neural Information Processing Systems (NeurIPS)*, 2019. URL https://proceedings.neurips.cc/paper/2019/hash/b6f97e6f0fd175613910d613d574d0cb-Abstract.html.

[30] Giuseppe Paolo, Alexandre Coninx, Stephane Doncieux, and Alban Laflaquière. Sparse reward exploration via novelty search and emitters. In *Proceedings of the Genetic and Evolutionary Computation Conference*, page 154–162, 2021. URL https://doi.org/10.1145/3449639.3459314.

[31] Cédric Colas, Pierre Fournier, Mohamed Chetouani, Olivier Sigaud, and Pierre-Yves Oudeyer. CURIOUS: Intrinsically motivated modular multi-goal reinforcement learning. In *International Conference on Machine Learning (ICML)*, 2019. URL https://proceedings.mlr.press/v97/colas19a.html.

[32] A.S. Klyubin, D. Polani, and C.L. Nehaniv. Empowerment: a universal agent-centric measure of control. In *IEEE Congress on Evolutionary Computation*, volume 1, pages 128–135 Vol.1, 2005. URL https://ieeexplore.ieee.org/document/1554676.

[33] Shakir Mohamed and Danilo Jimenez Rezende. Variational information maximisation for intrinsically motivated reinforcement learning. In *Advances in Neural Information Processing Systems (NeurIPS)*, 2015. URL https://arxiv.org/abs/1509.08731.

[34] Marc Bellemare, Sriram Srinivasan, Georg Ostrovski, Tom Schaul, David Saxton, and Remi Munos. Unifying count-based exploration and intrinsic motivation. *Advances in Neural Information Processing Systems (NeurIPS)*, 2016.

[35] Haoran Tang, Rein Houthooft, Davis Foote, Adam Stooke, OpenAI Xi Chen, Yan Duan, John Schulman, Filip DeTurck, and Pieter Abbeel. # exploration: A study of count-based exploration for deep reinforcement learning. *Advances in Neural Information Processing Systems (NeurIPS)*, 2017.

[36] Edward S. Hu, Richard Chang, Oleh Rybkin, and Dinesh Jayaraman. Planning goals for exploration. In *International Conference on Learning Representations (ICLR)*, 2023. URL https://openreview.net/forum?id=6qeBuZSo7Pr.

[37] Russell Mendonca, Oleh Rybkin, Kostas Daniilidis, Danijar Hafner, and Deepak Pathak. Discovering and achieving goals via world models. In *Advances in Neural Information Processing Systems (NeurIPS)*, 2021. URL https://openreview.net/forum?id=6vWuYzkp8d.

[38] OpenAI, Matthias Plappert, Raul Sampedro, Tao Xu, Ilge Akkaya, Vineet Kosaraju, Peter Welinder, Ruben D'Sa, Arthur Petron, Henrique Ponde de Oliveira Pinto, Alex Paino, Hyeonwoo Noh, Lilian Weng, Qiming Yuan, Casey Chu, and Wojciech Zaremba. Asymmetric self-play for automatic goal discovery in robotic manipulation. *arXiv:2101.04882*, 2021. URL https://arxiv.org/abs/2101.04882.

[39] John B. Lanier, Stephen McAleer, and Pierre Baldi. Curiosity-driven multi-criteria hindsight experience replay, 2019.

[40] Ashvin Nair, Bob McGrew, Marcin Andrychowicz, Wojciech Zaremba, and Pieter Abbeel. Overcoming exploration in reinforcement learning with demonstrations. In *2018 IEEE international conference on robotics and automation (ICRA)*, pages 6292–6299. IEEE, 2018.

[41] Ondrej Biza, Thomas Kipf, David Klee, Robert Platt, Jan-Willem van de Meent, and Lawson LS Wong. Factored world models for zero-shot generalization in robotic manipulation. *arXiv preprint arXiv:2202.05333*, 2022. URL https://arxiv.org/abs/2202.05333.

Supplementary Material for Regularity as Intrinsic Reward for Free Play

Code will be available at https://sites.google.com/view/rair-project.

A Experiment Results with Ground Truth Models

A.1 Experiment Results for RaIR in CONSTRUCTION with x-y-z

As discussed in Sec. 3.1, in our experiments we compute RaIR on the x-y subspace of the object positions in CONSTRUCTION to inject a bias towards vertical alignments. Examples of patterns generated when optimizing for RaIR using

$$\phi(s_i, s_j) = \{(|\lfloor s_{i,x} - s_{j,x} \rceil|, |\lfloor s_{i,y} - s_{j,y} \rceil|, |\lfloor s_{i,z} - s_{j,z} \rceil|)\}$$

are showcased in Fig. S10. When we also include the z-positions of the objects in the RaIR computation, patterns and constellations on the ground are preferred. In this case, there is no difference between a horizontal line on the ground vs. a vertical line, i.e. a stack. Since creating a stack, however, is a more sparse solution, in practice the zero-order trajectory optimizer converges already to regular structures on the ground and vertical constellations don't emerge. Starting from a randomly initialized scene with all objects on the ground, the regularity metric for x-y-z only starts increasing when multiple objects are in the stack, which would require a very long planning horizon to find this solution.

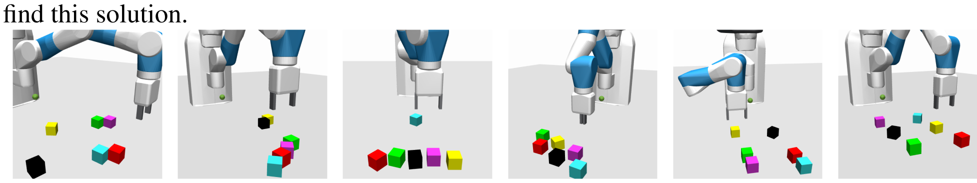

Figure S10: **Emerging patterns with RaIR on the x-y-z subspace with GT models**, where we use absolute relational ϕ.

B Experiment Results for Relational Case without Absolute Value

We present the interaction metrics observed during free play with RaIR + CEE-US in the case of relational ϕ with $\phi(s_i, s_j) = \{\lfloor s_i - s_j \rceil\} = \{(\lfloor s_{i,x} - s_{j,x} \rceil, \lfloor s_{i,y} - s_{j,y} \rceil)\}$. We find the interaction metrics to be comparable to the absolute relational case presented in the main paper with $\phi(s_i, s_j) = \{(|\lfloor s_{i,x} - s_{j,x} \rceil|, |\lfloor s_{i,y} - s_{j,y} \rceil|)\}$. In Fig. S11, we also include the results for RaIR + CEE-US with $\lambda = 1$. In the case of the increased weighting on the ensemble disagreement term, the free-play behavior indeed collapses back onto CEE-US. This means we have more flipping behavior and less air time. In the case of RaIR + CEE-US with smaller $\lambda = 0.1$, we seek regular states, which include vertical alignments, such that the air time doesn't go down. Note that in this case, there is still an incentive to "destroy" and lean towards chaos due to the ensemble disagreement reward term, such that the constellations showcased in Fig. 6 (snapshots for the absolute relational ϕ) and Fig. S12 are not necessarily preserved.

We also evaluate the success rates for zero-shot downstream task generalization using the models trained in free-play runs with relational (R) ϕ and present them in Table S3. We find the performance in this case to be comparable to the absolute relational (AR) ϕ case.

C Experiment Results for Free Play with pure RaIR

In this section, we present zero-shot downstream task generalization performance for free play with pure RaIR and further discuss the role of the information-gain term in our intrinsic reward combination used in free play, as specified in Eq. 6. As discussed in Sec. 3.2, adding ensemble disagreement to our regularity objective leads to 1) more interaction-rich free play and 2) more robust

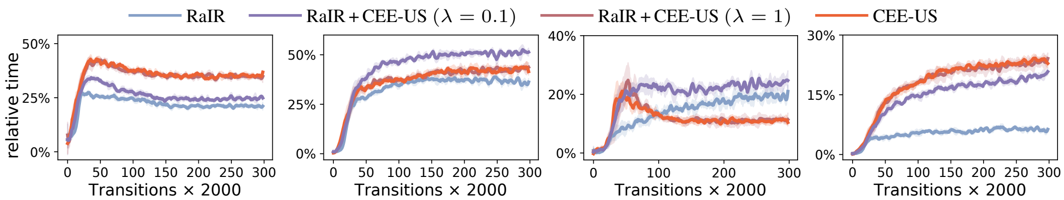

(a) 1 object moves (b) 2 or more objects move (c) object(s) in air (d) object(s) flipped

Figure S11: **Comparison of interactions during free play in CONSTRUCTION when combining ensemble disagreement with RaIR for different augmentation weights λ with relational ϕ.** Interaction metrics of free-play exploration count the relative amount of time steps spent in moving one object (a), moving two and more objects (b), moving objects in the air (d), and flipping object(s) (c). We used 5 independent seeds.

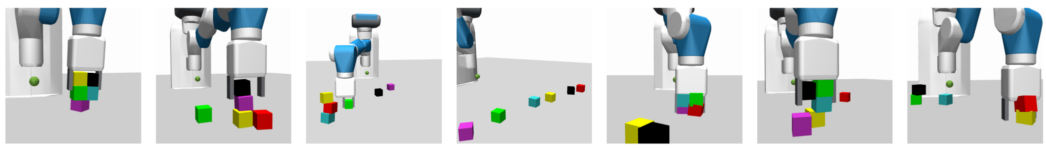

Iteration 245 Iteration 246 Iteration 247 Iteration 248 Iteration 270 Iteration 275 Iteration 295

Figure S12: **Snapshots from free play with RaIR + CEE-US and relational ϕ.** We showcase snapshots of lowest entropy from exemplary rollouts at different iterations of free play. Following the regularity objective, stacks and alignments are generated. These snapshots come from a run with $\lambda = 0.1$.

Table S3: **Zero-shot downstream task generalization performance of RaIR + CEE-US for different ϕ and λ** for assembly tasks as well as the generic pick & place task and the more chaos-oriented throwing and flipping. Results are shown for five independent seeds. AR: Absolute relative ϕ, R: Relative ϕ. In the bottom row, we report the success rates achieved via planning with ground truth models. This is to provide a baseline for how hard the task is to solve with finite-horizon planning and potentially suboptimally designed task rewards.

	Singletower 3	Multitower 2+2	Pyramid 5	Pyramid 6	Pick&Place 6	Throw 4	Flip 4
RaIR + CEE-US (R)	$\mathbf{0.80 \pm 0.07}$	$\mathbf{0.77 \pm 0.03}$	$\mathbf{0.47 \pm 0.04}$	$\mathbf{0.17 \pm 0.05}$	$\mathbf{0.90 \pm 0.01}$	0.38 ± 0.02	0.63 ± 0.05
RaIR + CEE-US (AR)	$\mathbf{0.75 \pm 0.07}$	$\mathbf{0.77 \pm 0.06}$	$\mathbf{0.49 \pm 0.06}$	$\mathbf{0.18 \pm 0.04}$	$\mathbf{0.90 \pm 0.02}$	0.32 ± 0.02	0.63 ± 0.08
RaIR (AR)	0.64 ± 0.03	0.62 ± 0.03	0.25 ± 0.05	0.10 ± 0.02	0.74 ± 0.05	0.21 ± 0.01	0.65 ± 0.1
CEE-US	0.40 ± 0.12	0.52 ± 0.05	0.14 ± 0.09	0.02 ± 0.01	$\mathbf{0.90 \pm 0.02}$	$\mathbf{0.49 \pm 0.05}$	$\mathbf{0.73 \pm 0.1}$
GT	0.99	0.97	0.82	0.81	0.99	0.97	1.0

world models which yield higher success rates for zero-shot downstream task generalization. For both the absolute relational case presented in Fig. 5 and the relational case in Fig. S11, RaIR with no disagreement term yields less interactions in terms of object(s) being moved, being in air and being flipped. This is because the exploration problem is not solved by RaIR alone. When we use ensemble disagreement as an intrinsic reward, the discovery of different types of interactions is accelerated. When one of the models in the ensemble learns a new type of dynamics, such as an object moving, the ensemble disagreement goes up, incentivizing the agent to repeat this behavior until it is learned by all models such that disagreement goes down. In the case of RaIR, this only happens implicitly: with some models in the ensemble learning a certain type of dynamics in the environment, during planning, the models can hallucinate objects being aligned and creating a regular pattern with high RaIR such that these actions are executed by the controller. These false attempts also help exploration.

As the models produce better predictions, especially after free play iteration 200, we observe that more stable patterns are generated with RaIR compared to RaIR + CEE-US and the amount of time objects are moving starts decreasing. This is because in this case when the models get better and hallucinate less, there is no reason to leave local optima such as a spaced line unless a pattern that yields a higher regularity value can be found within the planning horizon.

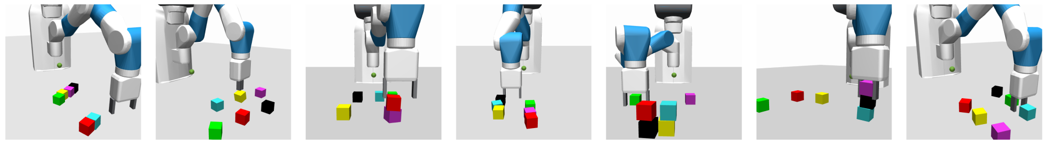

Figure S14: **Snapshots from free play with pure RaIR.** We showcase snapshots of lowest entropy from exemplary rollouts at different iterations of free play. These snapshots come from a run with absolute relational ϕ.

The challenge of exploration with pure RaIR is also reflected in the interaction time for object(s) in air. Starting to create regular patterns such as stacks takes longer, as exploring to lift objects happens later without the disagreement reward. This is also connected to the step-wise landscape of RaIR as discussed in Sec. 3.2 such that explicit exploration via ensemble disagreement is beneficial.

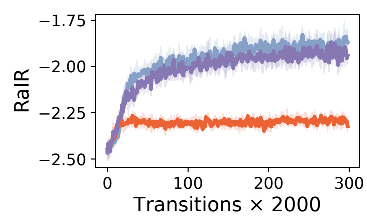

Figure S13: **Highest RaIR value throughout free play** for RaIR, RaIR + CEE-US and CEE-US.

As showcased in Fig. S14, we still observe the stable generation of patterns such as spaced lines later on in training as well, as these are local optima of RaIR. However, we start to see more stacks generated in the later stages of free play. In Fig. S13, the highest RaIR value achieved for the different variants are showcased throughout training. Pure RaIR, achieves slightly higher regularity then RaIR + CEE-US. This is also because pure RaIR, tends to generate more regular patterns that feature all objects, i.e. all objects are in-line or build a square. With RaIR + CEE-US, as some chaotic behavior is injected to free play via ensemble disagreement, more local regularities such as a stack of 2, with the rest of the objects in disorder, are likely to emerge.

Through injecting ensemble disagreement into free play, the robustness of the learned world models is also increased as they are guided by their own epistemic uncertainty [12]. During free play, data is actively collected from regions where the models are uncertain, acting as their own adversary. This in turn makes the models more robust for deployment in model-based planning in the follow-up extrinsic phase, where the accuracy of model predictions is paramount for good performance. This is reflected in the downstream task performance evaluations in Fig. S15, where RaIR + CEE-US consistently outperforms both RaIR and CEE-US in the assembly tasks. Note that as regularity explicitly favours alignments such as stacks, unlike CEE-US, these dynamics are explored better, leading to higher success rates. This also showcases the importance of guiding free play towards regularity. In Fig. S16, the results for the pick & place, throwing and flipping tasks are shown. Due to the increased robustness of the model with the disagreement term, we indeed observe better performance for RaIR + CEE-US and CEE-US for the Pick & Place task compared to pure RaIR. This is also true for the throwing task. However, another contributing factor here is that models with disagreement favor more chaotic behaviors and perform more “throwing”-like behaviors during free play. As CEE-US has no bias towards regularity, it performs best, whereas pure RaIR performs worse than RaIR + CEE-US. Interestingly, for the flipping 4 objects task we found performance for RaIR and RaIR + CEE-US to be comparable despite the significantly reduced amount of time spent flipping objects in the case of pure RaIR, as can be seen in Fig. 5. Upon inspecting the data generated during free-play, we hypothesize this is because unlike RaIR + CEE-US, which flips and rolls objects together in a chaotic way, we found RaIR to produce more isolated flipping of individual objects.

D Experiment Results for Re-creating Existing Patterns

As presented in Sec. 3.4, we test whether we can re-create existing regularities in the environment by simply optimizing for RaIR with iCEM, using ground truth models. As for the pyramid with 3 objects in Sec. 3.4, we initialize different regular structures outside of the robot’s manipulability range and test whether these regular patterns can be re-created, merely by maximizing for RaIR. We test for the re-creation of a singletower with 3 and 4 objects, 2 towers with 2 objects each (referred to as multitower 2+2), as well as a spaced line and a rhombus with 4 objects. We test this with ground truth models for 15 independent rollouts for each structure and report the re-creation rates. Example

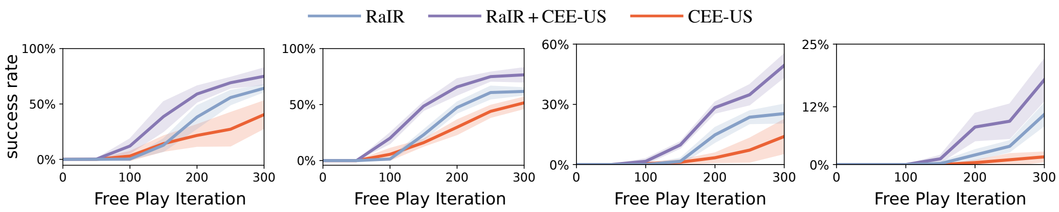

(a) Singletower 3 (b) Multitower 2+2 (c) Pyramid 5 (d) Pyramid 6

Figure S15: **Downstream task performance for assembly tasks** with only RaIR ($\lambda = 0$), RaIR + CEE-US ($\lambda = 0.1$) and CEE-US. We use absolute relational ϕ for RaIR computations.

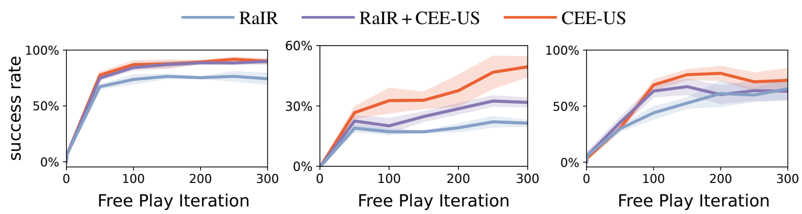

(a) Pick & Place 6 (b) Throw 4 (c) Flip 4

Figure S16: **Downstream Task Performance for Pick & Place and the more chaotic tasks of throwing and flipping** with only RaIR ($\lambda = 0$), RaIR + CEE-US ($\lambda = 0.1$) and CEE-US. We use absolute relational ϕ for RaIR computations.

rollouts are illustrated in Fig. S17. Note that due to the limited sample-budget with iCEM and the finite-horizon, we don't necessarily converge to the global minima, which corresponds to the full recreation of the structure. However, in all of the tested cases, the generated structures repeat at least one prominent sub-structure present in the underlying regular constellation by optimizing for RaIR.

For *Singletower 3*, the entire stack of 3 gets recreated 73% of the time. A partial recreation with a stack of 2 blocks is observed in all but one of the remaining cases.

When a *Singletower 4* is initialized outside of the robot's range, the full tower with 4 blocks gets recreated 40% of the time. In the remaining cases, either a tower of 3 (33%) or towers of 2 (27%) are built.

For the challenging *Multitower 2+2* case, the two towers are built, with the same distance to each other as in the original pattern, 20% of the time. An example of this "complete" recreation is illustrated in Fig. S17c. Otherwise, 53% of the time a stack of 2 is built (Fig. S17d) or a spaced line repeating the relative position of the two towers in the original pattern.

For the patterns on the ground, namely *Spaced Line* and *Rhombus*, the recreation rates are higher since the exploration problem is less prominent. At least 75% of the original pattern is re-created at each rollout, i.e. for the case of 4 objects, at least 3 objects follow the original pattern. The complete *Spaced Line* is recreated 80% and the entire rhombus 73% of the test rollouts.

In these experiments, we use RaIR with $\phi(s_i, s_j) = \{(|\lfloor s_{i,x} - s_{j,x} \rceil|, |\lfloor s_{i,y} - s_{j,y} \rceil|, |\lfloor s_{i,z} - s_{j,z} \rceil|)\}$. This is because in the case of existing structures in the scene, we don't need/want to inject any biases into the optimization. As the existing pattern is outside of the manipulability range of the robot, re-creating the pattern becomes a direct global optimum for RaIR, as all regularities reoccur. However, if we restrict ourselves to the x-y subspace, this is no longer the case: even for a rhombus, a stack built with the blocks in-reach becomes the global optimum. This is because all the blocks in the stack then have the same x-y relation to the blocks in the rhombus.

E CEE-US

In this section, we present the details of CEE-US [12], which we build upon in this work. CEE-US uses structured world models together with model-based planning during exploration, achieving increased sample-efficiency and superior downstream task performance compared to other intrinsically-

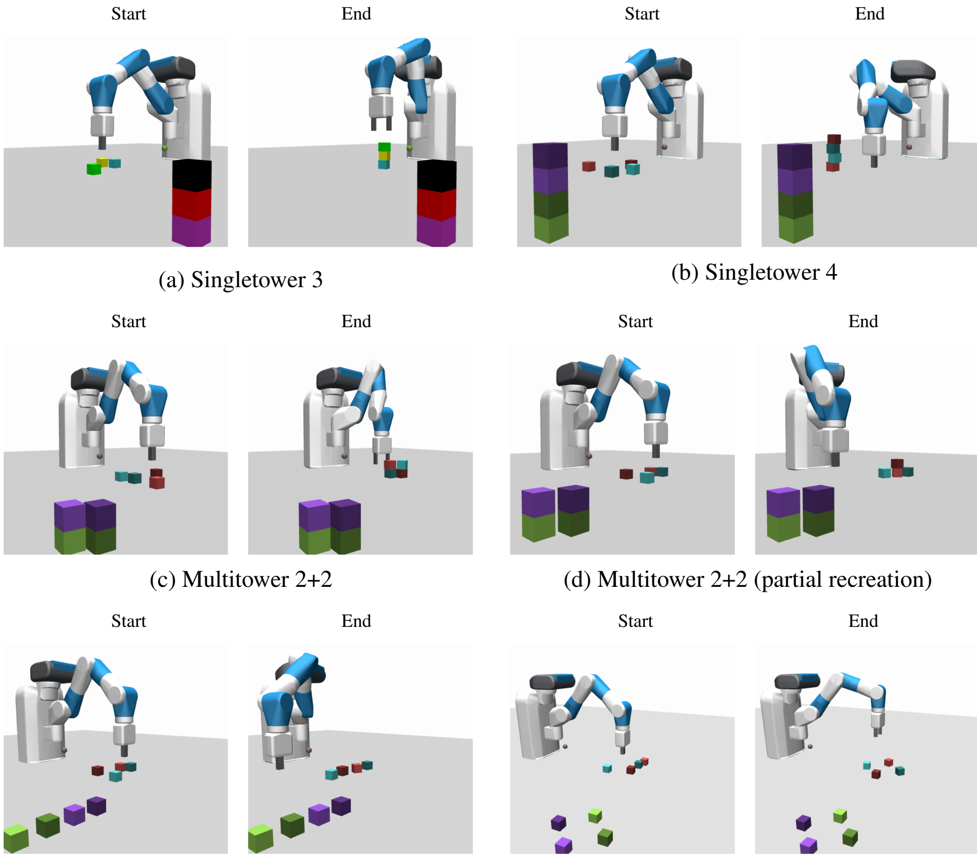

(a) Singletower 3 (b) Singletower 4

(c) Multitower 2+2 (d) Multitower 2+2 (partial recreation)

(e) Spaced line 4 (f) Rhombus 4

Figure S17: Different regular structures initialized outside of the robot's reach at the start of the episode ($t = 0$) and re-created by optimizing for RaIR with GT models. Showcased here for the end of the episode ($t = 200$).

motivated RL baselines. The free-play pseudocode is presented in Alg. S1. This free-play structure is used for all methods presented in our paper by swapping out the intrinsic reward term (line 5) with only ensemble disagreement (CEE-US), combination of our regularity objective with ensemble disagreement (RaIR + CEE-US) or pure regularity (RaIR).

Algorithm S1 Free Play in Intrinsic Phase (taken from [12])

1: **Input:** $\{(\tilde{f}_{\theta_m})_{m=1}^M\}$: Randomly initialized ensemble of GNNs with M members, D: empty dataset, `Planner`: iCEM planner with horizon H
2: **while** explore **do** ▷ *Explore with MPC and intrinsic reward*
3:   **for** $e = 1$ **to** `num_episodes` **do**
4:     **for** $t = 1$ **to** T **do** ▷ *Plan to maximize intrinsic reward*
5:       $a_t \leftarrow \texttt{Planner}(s_t, \{(\tilde{f}_{\theta_m})_{m=1}^M\}, r_{\text{intrinsic}})$ ▷ *e.g. RaIR with disagreement Eq. 6*
6:       $s_{t+1} \leftarrow \texttt{env.step}(s_t, a_t)$
7:     $\mathcal{D} \leftarrow \mathcal{D} \cup \{(s_t, a_t, s_{t+1})_{t=1}^T\}$
8:   **for** $l = 1$ **to** L **do** ▷ *Train models on dataset for L epochs*
9:     $\theta_m \leftarrow$ optimize θ_m using $\mathcal{L}_m$ on $\mathcal{D}$ for $m = 1, \ldots, M$
10: **return** $\{(\tilde{f}_{\theta_m})_{m=1}^M\}, \mathcal{D}$

E.1 GNN Architectural Details

Message-passing Graph Neural Networks (GNN) are deployed as world models. The same GNN architecture is used as in CEE-US [12]. For these structured world models, we consider object-factorized state spaces with $\mathcal{S} = (\mathcal{S}_{\text{obj}})^N \times \mathcal{S}_{\text{robot}}$. Each node in the GNN corresponds to an object and the robot/actuated agent is differentiated from the object nodes as a global node. The concatenation of the robots's state s_t^{robot} and the action a_t is represented as a global context $c = [s_t^{\text{robot}}, a_t]$. We have a fully-connected GNN. The node update function g_{node} and the edge update function g_{edge} model the dynamics of the entities/objects, and their pairwise interactions respectively. These functions are both Multilayer Perceptrons (MLP). In the following, we denote the state of the i-th object s_{t,obj_i} at timestep t as s_t^i for simplicity. The object node attributes in the GNN are updated as:

$$e_t^{(i,j)} = g_{\text{edge}}\big(\big[s_t^i, s_t^j, c\big]\big) \tag{S7}$$

$$\tilde{s}_{t+1}^i = g_{\text{node}}\big(\big[s_t^i, c, \operatorname{aggr}_{i \neq j}\left(e_t^{(i,j)}\right)\big]\big). \tag{S8}$$

where $[\cdot, \ldots]$ denotes concatenation, $e_t^{(i,j)}$ is the edge attribute between two neighboring nodes (i, j). For the permutation-invariant aggregation function given by aggr, we use the mean.

The robot state, which is treated as a global node, is computed using the global aggregation of all edges with a separate global node MLP g_{global}:

$$\tilde{s}_{t+1}^{\text{robot}} = g_{\text{global}}\big(\big[c, \operatorname{aggr}_{i,j}\left(e_t^{(i,j)}\right)\big]\big). \tag{S9}$$

Moreover, the GNN predicts the changes in the dynamics such that $\tilde{s}_{t+1} = s_t + \text{GNN}(s_t, a_t)$.

E.2 Planning Details

For planning, we use the improved Cross-Entropy Method (iCEM) [19]. The planner minimizes the cost, corresponding to negative reward $c(s_t, a_t, s_{t+1}) = -r(s_t, a_t, s_{t+1})$, where r can be intrinsic rewards $r_{\text{intrinsic}}$ or extrinsic task rewards r_{task}. The extrinsic task rewards are assumed to be given by the environment.

At each timestep t in the environment, the planner samples P action sequences, each with length H, i.e. the planning horizon. These actions are rolled out either in the ground truth model (perfect simulations) or in the imagination of a learned model (imperfect simulations), generating corresponding P state sequences with length H. In order to assign a cost to each of the P trajectories, we need to aggregate the cost over the horizon H. A typical choice here is `sum`, where the cost over the length of the trajectory is simply summed up: $\texttt{cost}^{(p)} = \sum_{h=0}^{H-1} c(s_{t+h}^{(p)}, a_{t+h}^{(p)}, s_{t+h+1}^{(p)})$.

However, this type of aggregation is not suitable for cases where a decrease in cost can in general be preceded by an initial increase. In these cases, using the mode `best`, that assigns the plan p the cost of the "best" timestep over the planning horizon with $\texttt{cost}^{(p)} = \min\Big(\{c(s_{t+h}^{(p)}, a_{t+h}^{(p)}, s_{t+h+1}^{(p)})\}_{h=0}^{H-1}\Big)$ is a better suited choice. We also empirically found this controller mode to be better at picking up *sparse* signals. What we mean here is that, in the example of stacking, it is hard to find a sampled trajectory that stacks the objects in a stable way with a limited sample-budget as this poses an exploration challenge. However, if we manage to find an action sequence that brings the cubes on top of each other, albeit in an unstable way, favoring this solution with `best` and keeping this solution in the elite set is beneficial. This can be explained as follows: In iCEM the K plans with the lowest assigned cost are chosen to be the elite set, which is then used to fit the sampling distribution of iCEM. As a fraction ξ of these elites is potentially shifted to the next internal iCEM iteration (`keep_elites`), and possibly to the next timestep (`shift_elites`), keeping these solutions that "fail" and yet bring us closer to the actual solution provides a better strategy to solve tasks which pose an exploration challenge such as stacking. Here, we are also relying on the fact that we are re-running optimization every timestep t in the environment with online model predictive control, such that we have the opportunity to correct these initially "wrong" solutions and find their "stable" counterparts. Note that this mode of the controller is a more unstable mode compared to `sum`. Especially with imperfect world models, where the model can hallucinate as the model errors accumulate over the planning horizon, mode `best` can pick up these falsely imagined future states with low cost. It also doesn't account for the fact that the planned trajectory keeps the lowest cost over multiple timesteps, such that a trajectory where an object flies through the goal location for a single timestep has the same cost as a trajectory where the object lands in the goal position and stays there. To account for this, we use $\texttt{cost}^{(p)} = \min\Big(\{c(s_{t+h}^{(p)}, a_{t+h}^{(p)}, s_{t+h+1}^{(p)})\}_{h=1}^{H-1}\Big)$, where we don't take into account the first timestep of the plan with $h = 0$. Although this is not a robust solution, we found it to empirically work well. Quantitatively, stacking 3 objects when planning with ground truth models yields 99% success rate for mode `best`, whereas only 47 % success rate for `sum`, using the same reward function in both cases. Even in the case of perfect dynamics predictions with GT models, this showcases the importance of the controller mode to be able solve tasks with sparse reward signals.

F Experiment Details

In this section, we provide experimental details and hyperparameter settings.

F.1 Environment Details

SHAPEGRIDWORLD This is a discrete 2D grid, where each entity/agent is controlled individually in the x-y directions. This means entities are controlled one at a time and actuation keeps iterating over the entities, where we use an object persistency of 10 timesteps. The action a_t is 2 dimensional, controlling the agent in x-y directions separately and is applied on the current actuated entity i in the grid. As we are operating in a discrete grid, the actions are actually discrete such that the agent can move one grid cell to the left/right and up/right (if the target grid cell is not occupied) or stay at the current grid cell. The first dimension of the action controls agent movement in x- and the second dimension in the y-direction. In order to make this environment work with the default iCEM implementation with a Gaussian sampling distribution, we perform a discretization step before inputting the sampled actions to the environment. For the experiment results with GT models presented in Fig. 1, we use a grid size of 25×25 with 16 and 32 objects.

CONSTRUCTION This is a multi-object manipulation environment as an extension of the Fetch Pick & Place environment proposed in [24]. We also applied the two modifications from Sancaktar et al. [12]. 1) The table in front of the robot is replaced with a large plane such that objects cannot fall off during free play, but can still be thrown/pushed outside of the robot's reach. 2) In Li et al. [24], the object state also contained the object's position relative to the gripper which was removed, as it already introduces a relational bias in the raw state representation. Details on the dimensionalities of the object and robot state spaces can be found in Table S5.

F.2 Parameters for Ground Truth Model Experiments with RaIR

The controller parameters used when optimizing RaIR with ground truth (GT) models are given in Table S4. To compute RaIR, we perform a discretization step in the CONSTRUCTION environment as it is continuous. For GT models, that produce perfect mental simulations, we can choose a small bin size of 1cm. In comparison, the size of one block in the environment is 5 cm. The bin size also gives us the upper bound of the *regularity precision* that can be achieved during optimization, e.g. a perfectly aligned stack vs. a zigzagged stack. Note however that the higher the precision is, the harder it typically gets for the controller to converge to global optima with a horizon of 30 timesteps and a limited sample-budget.

As discussed in Sec. A, this is also a constraint when we are computing RaIR in the x-y-z subspace. Due to this, for the re-creation of existing patterns experiments presented in Sec. 3.4 and Sec. D, we compute RaIR with a bin size of 2.5cm and increase the number of sampled trajectories P to 512. Although we could further increase the bin size, we choose this value to not negatively impact the precision of the re-created structures.

F.3 Free Play with Learned Models

The environment properties with the episode lengths and model training frequencies are given in Table S5. Six objects are present in CONSTRUCTION during free play. The parameters for the GNN model architecture as well as the training parameters for model learning are listed in Table S6. For the RaIR computations in free play, we use a bin size of 5cm, which is equivalent to the size of a block.

The set of the hyperparameters for the iCEM controller used in the intrinsic phase of RaIR + CEE-US, RaIR and CEE-US are the same as presented in Table S4. The only difference to the GT model case is, we use a planning horizon of 20 timesteps for free play.

Table S4: Base settings for iCEM. These hyperparameters are used when using GT models to optimize RaIR.

(a) General settings.

Parameter	Value
Number of samples P	128
Horizon H	30
Size of elite-set K	10
Colored-noise exponent β	3.5
CEM-iterations	3
Noise strength σ_{init}	0.5
Momentum α	0.1
`use_mean_actions`	Yes
`shift_elites`	Yes
`keep_elites`	Yes
Fraction of elites reused ξ	0.3
Cost along trajectory	`best`

(b) Environment-specific settings.

SHAPEGRIDWORLD	
Parameter	**Value**
Number of samples P	64

CONSTRUCTION	
Parameter	**Value**
Same as general settings	

Table S5: Environment settings for CONSTRUCTION. 2000 transitions (20 episodes with 100 timesteps each) are generated within one iteration of free play.

CONSTRUCTION	
Parameter	**Value**
Episode Length	100
Train Model Every	20 Episodes
Action Dim.	4
Robot/Agent State Dim.	10
Object Dynamic State Dim.	12
Num. of Objects During Free Play	6

Table S6: Settings for GNN model training in intrinsic phase of RaIR + CEE-US and CEE-US. (Same as in [12])

Parameter	Value
Network Size of g_{node}	2×128
Network Size of g_{edge}	2×128
Network Size of g_{global}	2×128
Activation function	ReLU
Layer Normalization	Yes
Number of Message-Passing	1
Ensemble Size	5
Optimizer	ADAM
Batch Size	125
Epochs	25
Learning Rate	10^{-5}
Weight Decay	0.001
Weight Initialization	Truncated Normal
Normalize Input	Yes
Normalize Output	Yes
Predict Delta	Yes

Table S7: Settings for the iCEM controller used for zero-shot generalization in the extrinsic phase of RaIR + CEE-US and CEE-US. The settings not specified here are the same as the general settings given in Table S4. The settings are exactly the same as in [12].

Task	Controller Parameters				
	Horizon h	Colored-noise exponent β	`use_mean_actions`	Noise strength σ_{init}	Cost Along Trajectory
CONSTRUCTION-Stacking	30	3.5	No	0.5	`best`
CONSTRUCTION-Pick & Place	30	3.5	Yes	0.5	`best`
CONSTRUCTION-Throwing	35	2.0	Yes	0.5	`sum`
CONSTRUCTION-Flipping	30	3.5	No	0.5	`sum`

F.4 Extrinsic Phase: Zero-shot Downstream Task Generalization

In this section, we provide details on the extrinsic phase following free play, where the learned GNN ensemble is used to solve downstream tasks zero-shot via model-based planning.

F.4.1 Details on Downstream Tasks and Reward Functions

The reward functions for all the downstream tasks are computed as specified in Sancaktar et al. [12], where for all the assembly tasks we use the same structure as in the stacking reward. However, we do one modification to the original reward computation in the assembly tasks. The assembly task reward is sparse incremental with reward shaping, where the reward also contains the distance between the gripper and the position of the next block to be stacked. We modify how the next block ID is computed in the original implementation from Sancaktar et al. [12]. Instead of naively checking the number of unsolved objects to obtain the next block ID irrespective of order, we determine the next block to be the next unsolved block in the order. We found this modification to be important especially for the Pyramid tasks, where the sub-optimal next block computation might lead to the agent receiving a reward to be close to the wrong block, in the case the robot places blocks with $i >$ `next_block_id` to their goal locations with just the sparse reward.

F.4.2 Planning Details for Downstream Tasks

The controller settings for the different downstream tasks are shown in Table S7, which are the same settings used in [12].

G Connections between Compression and RaIR

Our regularity objective, that seeks out low-entropy states with high redundancy, shares close ties with compression, and specifically with lossless compression using entropy coding.

We implemented a version of our regularity idea using the lossless compression algorithm `bzip2` corresponding to the direct version of RaIR with order $k = 1$ (Sec. 2.2). In this case, we describe the state s directly by the properties of each of the entities and the function $\phi : \mathcal{S}_{\text{obj}} \to \{\mathcal{X}\}^+$, that maps each entity to a set of symbols and obtain $\Phi(s) = \Uplus_{i=1}^{N} \phi(s_{\text{obj},i})$ as a union of all symbols for N objects. Instead of computing the entropy for the frequencies of occurrence in the resulting multiset of symbols like in RaIR, we instead transform these symbols into bytes and compress them with `bzip2`. We then define the intrinsic reward for compression as the negative length of the compressed ByteString such that:

$$r_{\text{compression}} = -\operatorname{len}(\texttt{bzip2.compress}(\{\Uplus_{i=1}^{N} \phi(s_{\text{obj},i})\}^+\texttt{.tobytes()})). \tag{S10}$$

We also managed to create regular shapes and patterns when optimizing for $r_{\text{compression}}$ via planning with ground truth models and also for free play with learned models. The reason we chose not to pursue this direction was because 1) lossless compression algorithms like `bzip2` don't perform as well on short ByteStrings, which is the case for us, as e.g. in CONSTRUCTION, we compress only 6 objects with their corresponding x-y positions, 2) artifacts are introducted to the regularity/compression metric by the transformation into bytes, where certain symbols become more compressible than others in this representation without any added regularity. As a result, we preferred our formulation with RaIR as it provides better control over the generated patterns and structures.

H Code and Compute

Code will be available on the project webpage `https://sites.google.com/view/rair-project`.

We run the ground truth model experiments on CPUs. As we are using the true environment simulator as a model, each imagination step in the planning horizon takes as long as an environment step. We parallelize the ground truth models on 16 virtual cores The controller frequency in this case is ca. $0.25\,\mathrm{Hz}$, for the settings given in Table S4.

For the free-play phase, we have a fixed number of transitions collected at each free play iteration, which get added to the replay buffer. After the data collection, the model is trained on the whole replay buffer for 25 epochs. Since the buffer size increases at each free play iteration with newly collected data, for this fixed number of epochs, the corresponding number of model training updates and thus also the runtime of the iteration, increase throughout free play. For RaIR + CEE-US, the full free-play (300 free play iterations) in CONSTRUCTION with 6 objects, where overall 600K data points are collected, takes roughly 87 hours using a single GPU (NVIDIA GeForce RTX 3060) and 6 cores on an AMD Ryzen 9 5900X Processor. The majority of this time is spent on the model training after data collection. The controller frequency for the collected rollouts with RaIR and the epistemic uncertainty calculations using a GNN ensemble is ca. $5\,\mathrm{Hz}$.